Physicochem. Probl. Miner. Process., 62(4), 2026, 225397

http://www.journalssystem.com/ppmp

Physicochemical Problems of Mineral Processing

ISSN 1643-1049

Effect of calcium carbonate and sodium carbonate on phosphorus transformation during iron ore reduction

Shichao Wu, Haipei Zhang, Bo Li, Zuyin Huang, Yonggang Wei, Haoyuan Xu

[1] Faculty of Metallurgical and Energy Engineering, Kunming University of Science and Technology, Kunming, 650093, China

[2] State Key Laboratory of Complex Nonferrous Metal Resources Clean Utilization, Kunming University of Science and Technology, Kunming 650093, China

Corresponding authors: 510268053@qq.com (Haipei Zhang); libokmust@163.com (Bo Li)

Abstract: Compared with other processes, the direct reduction-magnetic separation process can achieve the removal of lattice phosphorus in the iron minerals of high-phosphorus iron ore. Compared with a single phosphorus removal agent, when using sodium carbonate and calcium carbonate as a combined phosphorus removal agent, it has the advantages of low dosage and good phosphorus removal effect. However, the intrinsic relationship between phosphorus transformation and iron mineral reduction has not been revealed. This paper studied the influence of calcium carbonate and sodium carbonate on the phosphorus reaction process. The results showed that the addition of calcium carbonate and sodium carbonate reacts with the silicon components in the high-phosphorus sample to form calcium silicate, preventing the reduction of the apatite that has been formed. At a reduction temperature of 1200 ℃ and a reduction time of 5 min, the phosphorus in the iron minerals enters the gangue phase when the iron minerals are reduced to wustite, and prolonging the time further promotes the formation of metallic iron and the growth of metallic iron particles. This result provides a theoretical basis for the efficient utilization of iron minerals with lattice phosphorus.

***Keywords*:** high-phosphorus iron ore, phosphorus in iron minerals, calcium carbonate and sodium carbonate, direct reduction, transformation process

1. Introduction

The global reserves of high-phosphorus iron ore exceed 20 billion tons and are widely distributed in western Hubei of China, North Africa, Central Asia, and North America (Hu et al., 2026; Ji et al., 2025). Its unique structure results in the fine-grained intermingling of iron minerals and phosphorus minerals (Li et al., 2025), and some phosphorus is solid-solved in the lattice of iron minerals in a similar-atom form, making its utilization difficult. China's dependence on iron ore imports exceeds 80%, and the development of such massive resources can solve the shortage of high-grade iron ore in China (Dong e al., 2024; Ye et al., 2024; Singh et al., 2024).

Regarding dephosphorization processes for high-phosphorus iron ore, flotation, magnetic separation, and their combinations yield iron recoveries below 70% for finely disseminated iron ores, and most dephosphorization rates are less than 75% (Xiao and Zhou, 2019; You et al., 2024; Liu et al., 2026; Zhou et al., 2024; Zhang et al., 2025). Although hydrometallurgical leaching can achieve dephosphorization rates above 90%, it consumes up to 300 kg of acid per ton of ore and generates acidic wastewater (Guo et al., 2015). Bioleaching requires a cycle of 60–90 days and the bacterial strains exhibit poor adaptability to different ores (Jia et al., 2024). The pre-reduction and smelting separation process has high energy consumption (Silva et al., 2022), and the phosphorus content of the resulting iron product fluctuates between 0.15% and 0.35%. By contrast, the direct reduction-magnetic separation process can simultaneously achieve iron metallization and phosphorus fixation, showing promising iron recovery and dephosphorization effects (Zhao et al., 2024; Zhao et al., 2026; Liu et al., 2025; Yu et al., 2025). In this process, the addition of dephosphorization agents can enhance the reduction of iron

DOI: 10.37190/ppmp/225397

minerals, promote the growth of metallic iron particles, and inhibit the reduction of phosphorus minerals (Ji et al., 2025; Pownceby et al., 2019; Wu et al., 2026; Ding et al., 2023). However, current studies mainly focus on high-phosphorus iron ores where phosphorus occurs in the form of apatite (Zhu et al., 2013; Wang et al., 2025).

For a certain high-phosphorus iron ore, phosphorus occurs both in apatite and in the crystal lattice of iron minerals (Wu et al., 2023). Experimental results show that, among single dephosphorization agents, sodium carbonate yields the best dephosphorization rate, followed by calcium carbonate, while calcium fluoride gives the poorest rate (Wu et al., 2022). Compared with single agents, the combined dephosphorization agent of calcium carbonate and sodium carbonate achieves a higher dephosphorization rate at a lower dosage (Wu et al. 2021). Under the conditions of a $CaCO_3$: Na_2CO_3 mass ratio of 13:2, a total dephosphorization agent dosage of 15%, straw charcoal dosage of 15%, reduction temperature of 1200 °C, and reduction time of 70 min, a direct reduced iron product with an iron grade of 93.24%, iron recovery of 90.90%, and phosphorus content of 0.09% was obtained. However, the removal process of phosphorus from the iron minerals remains unclear, and the temperature and time required for phosphorus removal from the iron minerals have not been studied.

To address the above problems, a two-stage grinding and two-stage low-intensity magnetic separation method is adopted to prepare a high-phosphorus sample free of apatite. Among them, the fineness of the first stage grinding was -0.045mm, with a content of 85.51%; the fineness of the second stage grinding was -0.038mm, accounting for 95.80%. The magnetic separation field strength was all 800 Oe. X-ray diffraction (XRD) and scanning electron microscopy-energy dispersive spectroscopy (SEM–EDS) are employed to reveal the migration trajectory of phosphorus from the iron minerals during direct reduction under the action of calcium carbonate and sodium carbonate, and to investigate the migration behavior and transformation mechanism of phosphorus from the iron minerals at different temperatures and for different reduction times. The research results provide a theoretical basis for the clean utilization of phosphorus-bearing iron ores.

2. Materials and methods

2.1. Raw materials

The iron content of the high-phosphorus iron ore is 55.58%, and the phosphorus content is 0.57%. The main impurity components are SiO_2, Al_2O_3 and CaO, with their contents being 6.71%, 4.80% and 2.13% respectively. Fig. 1 and Table 1 show that the iron content in the high-phosphorus sample has significantly increased, with the iron content rising by 9.32 percentage points to reach 64.90%. In the high-phosphorus sample obtained by weak magnetic separation, the contents of almost all impurities have decreased. Among them, the content of SiO_2 has decreased significantly, from 6.71% to 1.82%. The content of Al_2O_3 has decreased from 4.80% to 2.73%, indicating that after magnetic separation, the high-phosphorus iron ore still contains a certain amount of aluminum and silicon. The content of CaO has decreased from 2.13% to 1.08%. It can be preliminarily inferred that the iron minerals contain phosphorus, because compared with the high-phosphorus oolitic hematite, the phosphorus content of the high-phosphorus sample decreased very little. Its main crystalline phases are magnetite and hematite, along with minor amounts of calcite and chlorite, which were not detected by XRD due to their low contents. The occurrence mode of phosphorus was investigated, and the results are shown in Fig. 2. The phosphorus distribution is basically uniform, and the area where phosphorus is distributed largely overlaps with the area where iron is distributed, indicating that phosphorus is distributed within the iron minerals. This confirms that even when magnified to the micrometer level, no phosphorus-enriched areas can be seen. It also confirms that there is no phosphorus existing as a separate mineral within the iron minerals, and phosphorus exists in the iron minerals in a similar composition form. This is consistent with the previous study (Wu et al., 2022).

The reducing agent is straw charcoal, and its fixed carbon, moisture, ash and volatile matter are 80.12%, 9.82%, 3.80% and 6.26% respectively. The chemical composition of its ash is shown in Table 2. It can be seen that the main components in the ash are SiO_2, Al_2O_3, Fe_2O_3, CaO and MgO, and their contents are 83.45%, 6.34%, 3.09%, 2.77% and 1.57% respectively. Analytical grade calcium carbonate and sodium carbonate were used as additives in this study.

Table 1. Chemical composition of high phosphorus sample/%

Contents	TFe	SiO_2	Al_2O_3	CaO	MgO	MnO	P	S
High phosphorus sample	64.90	1.82	2.73	1.05	0.30	0.18	0.49	0.011

Table 2. Chemical composition of the ash content of straw charcoal (wt%).

Component	SiO_2	Al_2O_3	Fe_2O_3	CaO	MgO	TiO_2	Na_2O	S
Ash	83.45	6.34	3.09	2.77	1.57	0.12	0.53	0.17

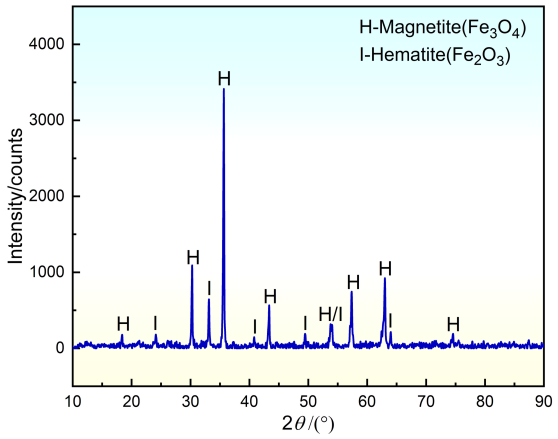

Fig. 1. Mineral composition of high phosphorus sample

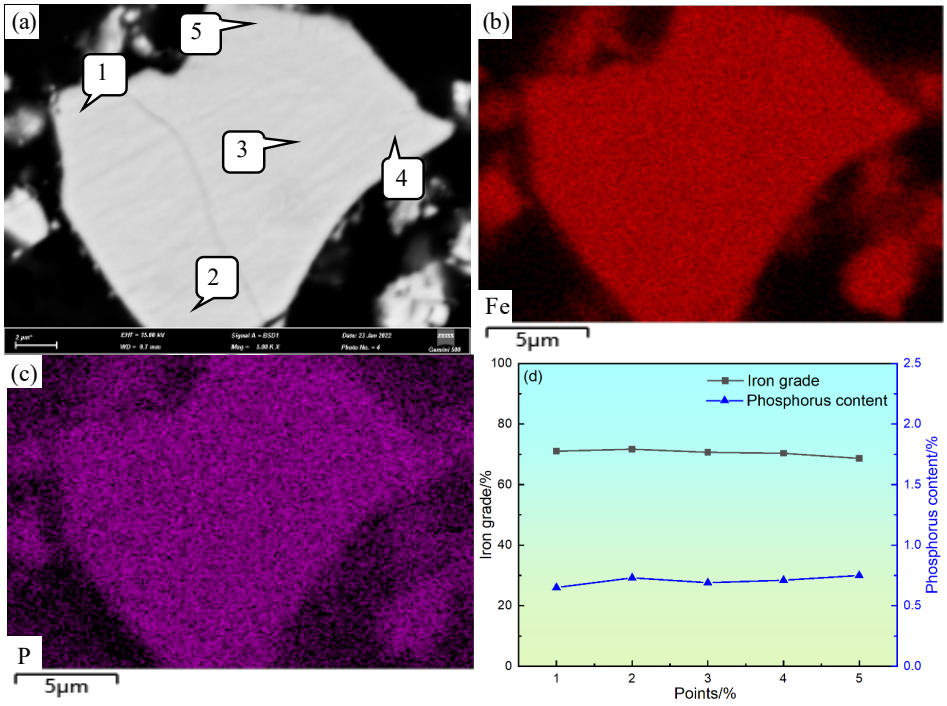

Fig. 2. Distribution characteristics of phosphorus in high-phosphorus sample: (a) Microstructure; (b) Iron distribution; (c) Phosphorus distribution; (d) Contents of phosphorus and iron

2.2. Experimental methods

2.2.1. Direct reduction

The high-phosphorus sample weighing 20 g was first thoroughly homogenized with appropriate amounts of straw charcoal, calcium carbonate, and sodium carbonate by manual grinding in an agate

mortar to ensure a uniform distribution of the additives. The resulting mixture was then quantitatively transferred into a clay crucible and lightly tamped to eliminate any entrapped air. After the muffle furnace had been preheated to the preset target temperature and allowed to stabilize for at least 15 min to ensure a uniform thermal field, the crucible was swiftly introduced into the hot zone of the furnace and maintained at that temperature for the predetermined reduction time. Immediately upon completion of the reduction cycle, the crucible was withdrawn from the furnace and the hot product was rapidly quenched by submerging it in a sufficient volume of cold running water to arrest any further reactions. The quenched solid was then recovered by filtration, and the resulting filter cake was transferred to a forced-air drying oven set at 105 °C, where it was kept for 2 h until constant weight was achieved, yielding the final reduced product ready for subsequent characterization.

2.2.2. Analysis and characterization

Thermodynamic calculations were performed using FactSage. The mineral composition of different reduced products was analyzed by X-ray diffraction (XRD), and the occurrence mode of phosphorus was studied using scanning electron microscopy coupled with energy dispersive spectroscopy (SEM–EDS).

3. Results and analysis

3.1. Thermodynamic analysis

FactSage was used to investigate the possible reactions occurring in the high-phosphorus sample with the addition of calcium carbonate and sodium carbonate, and the results are shown in Fig. 3. From Fig. 3(a), it can be seen that at 1200 °C, the Gibbs free energies of all reactions except reaction (2) are negative, indicating that with the addition of calcium carbonate and sodium carbonate, calcium carbonate reacts with silica to form dicalcium silicate, preventing the reduction of apatite formed at high temperature. In addition, calcium carbonate reacts with alumina to form tricalcium aluminate, and sodium carbonate reacts with silica and alumina to form nepheline, promoting the reduction of iron oxides. Fig. 3(b) shows that in the temperature range of 800 °C to 1200 °C, when the volume fraction of carbon monoxide exceeds 75%, reactions (7) to (9) all occur. Therefore, the addition of the combined dephosphorization agent can theoretically prevent the reduction of phosphorus.

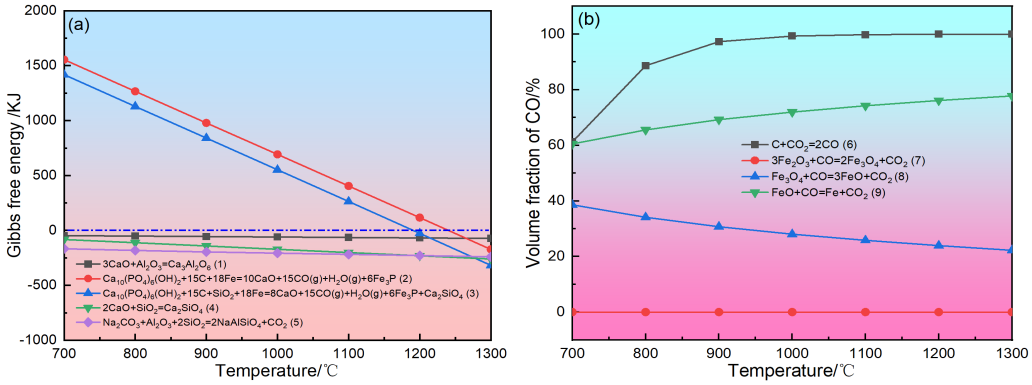

Fig. 3. Thermodynamic analysis: (a) Gibbs free energy; (b) Reduction process of iron minerals

3.2. Transformation process of phosphorus under different $CaCO_3$-to-Na_2CO_3 mass ratios

According to previous studies, under the conditions of 15% combined dephosphorization agent, 15% straw charcoal, reduction temperature of 1200 °C, and reduction time of 70 min, XRD was used to analyze the mineral composition of the reduced products at different ratios of calcium carbonate to sodium carbonate. The results are shown in Fig. 4. When the ratio of calcium carbonate to sodium carbonate was 15:0, the main minerals in the reduced product were metallic iron, calcium silicate, and tricalcium aluminate, indicating that the iron minerals were reduced to metallic iron, and calcium carbonate reacted with the silica and alumina components to form calcium silicate and tricalcium aluminate, respectively. When the ratio of calcium carbonate to sodium carbonate changed from 15:0 to

13:2, the mineral composition of the reduced product remained unchanged. When the ratio of calcium carbonate to sodium carbonate changed from 13:2 to 11:4, in addition to metallic iron, calcium silicate, and tricalcium aluminate, diffraction peaks of sodium calcium silicate appeared in the reduced product. When the ratio of calcium carbonate to sodium carbonate changed from 11:4 to 7:9, the mineral composition of the reduced product remained unchanged.

The analysis of the reduction products under different ratios of calcium carbonate to sodium carbonate was conducted using SEM–EDS, and the results are shown in Fig. 5. When the ratio of calcium

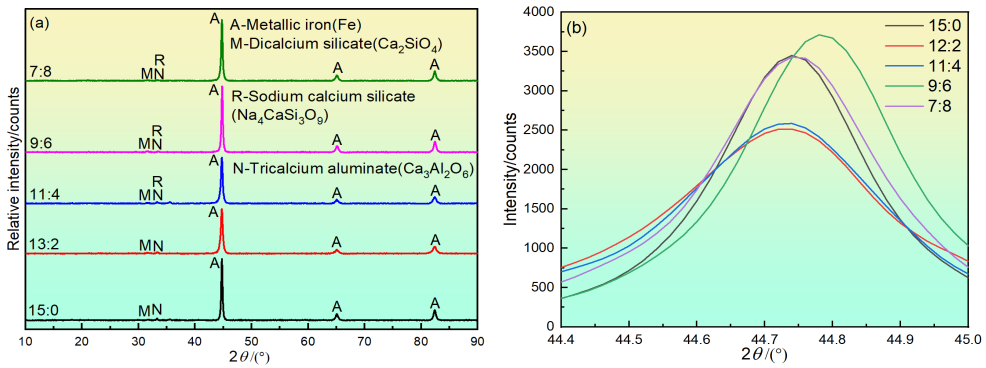

Fig. 4. Mineral composition of reduced products under different mass ratios of calcium carbonate to sodium carbonate: (a) Mineral composition; (b) Comparison of iron diffraction peaks

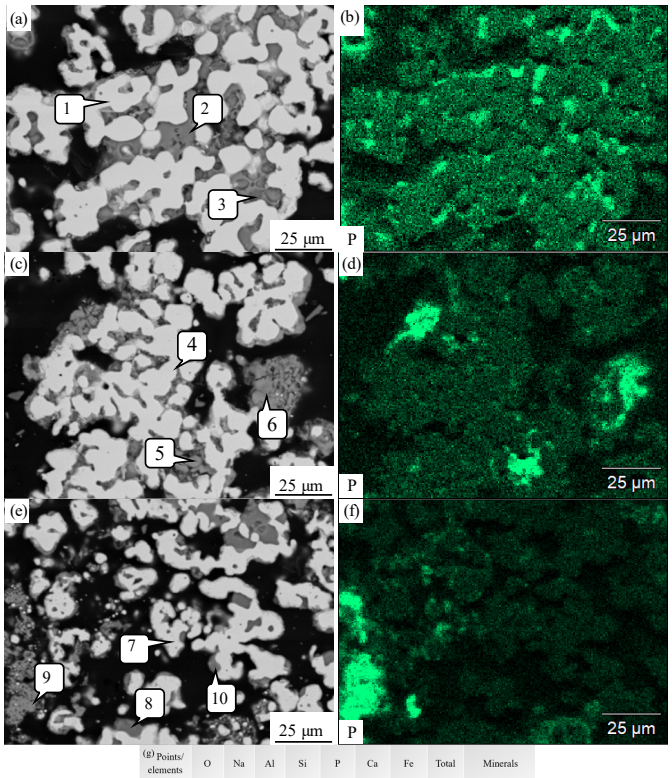

(g) Points/elements	O	Na	Al	Si	P	Ca	Fe	Total	Minerals
1	-	-	-	-	-	-	100.00	100.00	Metallic iron
2	41.07	-	-	9.43	4.24	45.26	-	100.00	Dicalcium silicate
3	37.30	-	-	-	17.38	45.32	-	100.00	Apatite
4	-	-	-	-	-	-	100.00	100.00	Metallic iron
5	43.32	1.67	-	10.63	4.04	40.34	-	100.00	Dicalcium silicate
6	37.62	-	-	-	19.83	42.55	-	100.00	Apatite
7	-	-	-	-	-	-	100.00	100.00	Metallic iron
8	43.74	1.34	-	8.46	3.99	42.47	-	100.00	Dicalcium silicate
9	35.91	-	-	-	20.53	43.56	-	100.00	Apatite
10	45.47	7.69	16.70	15.34	-	14.80	-	100.00	Sodium calcium silicate

Fig. 5. Occurrence states of phosphorus in reduced products under different mass ratios of calcium carbonate to sodium carbonate: (a) 15:0; (c) 13:2; (e) 7:8; (b), (d), (f) Respectively represent the phosphorus distribution in (a), (c), (e); (g) Mass percentages of each element from point 1 to point 10

carbonate to sodium carbonate was 15:0, the distributions of phosphorus and metallic iron did not overlap. Metallic iron was free of phosphorus, and phosphorus was mainly present in apatite. This indicates that when only calcium carbonate was added, the phosphorus in the iron minerals reacted with calcite to form apatite, which was then not reduced. When the ratio of calcium carbonate to sodium carbonate was 13:2, the occurrence state of phosphorus remained unchanged. When the ratio of calcium carbonate to sodium carbonate was 7:8, phosphorus was still present in apatite. It can also be observed that as the proportion of sodium carbonate increased, apatite became more concentrated, and the boundary between apatite and metallic iron became clearer, which is more favorable for the liberation of metallic iron grains during the subsequent grinding stage, thus facilitating dephosphorization.

3.3. Transformation process of phosphorus under different total dosages of $CaCO_3$ and Na_2CO_3

The mass ratio of calcium carbonate to sodium carbonate was fixed at 13:2. XRD was used to analyze the mineral composition of the reduction products under different dosages of calcium carbonate and sodium carbonate, and the results are shown in Fig. 6. When no calcium carbonate or sodium carbonate was added, diffraction peaks of metallic iron and hercynite were detected in the reduced product. At a total dosage of 3% calcium carbonate and sodium carbonate, the diffraction peak intensity of metallic iron increased, and peaks corresponding to calcium silicate and tricalcium aluminate appeared. When the total dosage was increased to 15%, the diffraction peak intensities of metallic iron, calcium silicate, and tricalcium aluminate all increased, confirming that calcium carbonate and sodium carbonate reacted with the silica and alumina components from chlorite and iron minerals to form dicalcium silicate and tricalcium aluminate, respectively, enhancing the diffraction peak intensity of metallic iron.

The reduced products obtained with different total dosages of calcium carbonate and sodium carbonate were analyzed by SEM–EDS, and the results are shown in Fig. 7. When no calcium carbonate or sodium carbonate was added, the distributions of phosphorus and metallic iron overlapped, and the metallic iron particles contained phosphorus, indicating that the free silica generated from the reduction of fayalite promoted the reduction of the apatite formed, and the resulting elemental phosphorus reacted with metallic iron to form an iron-phosphorus alloy. When the total dosage of calcium carbonate and sodium carbonate was 9%, metallic iron was free of phosphorus, and phosphorus was mainly present in apatite. This indicates that calcium carbonate and sodium carbonate reacted with the silica from chlorite and the silicon from iron minerals to form calcium silicate, thereby preventing the formation of free silica and thus inhibiting the reduction of the apatite formed. When the total dosage was increased to 15%, the occurrence state of phosphorus remained unchanged. As can be seen from the phase diagram in Fig. 7(h), in the absence of calcium oxide, the iron-phosphorus alloy is readily formed. The addition of calcium oxide prevents the formation of the iron-phosphorus alloy.

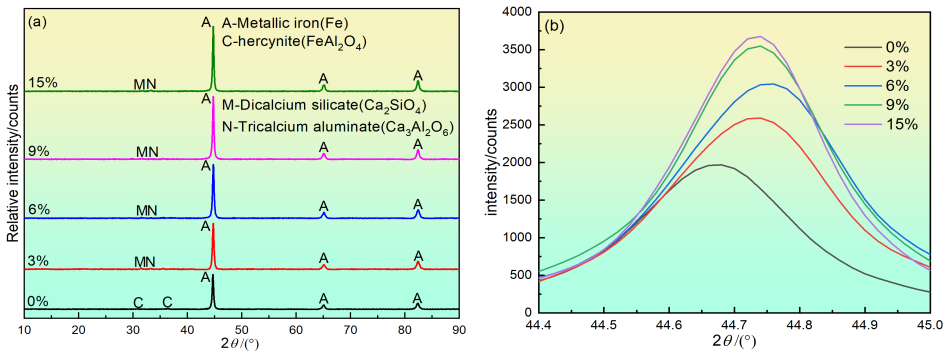

Fig. 6. Mineral composition of reduced products under different conditions: (a) Mineral composition; (b) Comparison of iron diffraction peaks

3.4. Reaction pathway of phosphorus under different reduction temperatures

The mineral composition of the reduced products obtained at different temperatures was analyzed by XRD, and the results are shown in Fig. 8. At a reduction temperature of 800 °C, the reduced product was mainly composed of magnetite, with minor amounts of hematite and calcite. At this stage, the iron mine-

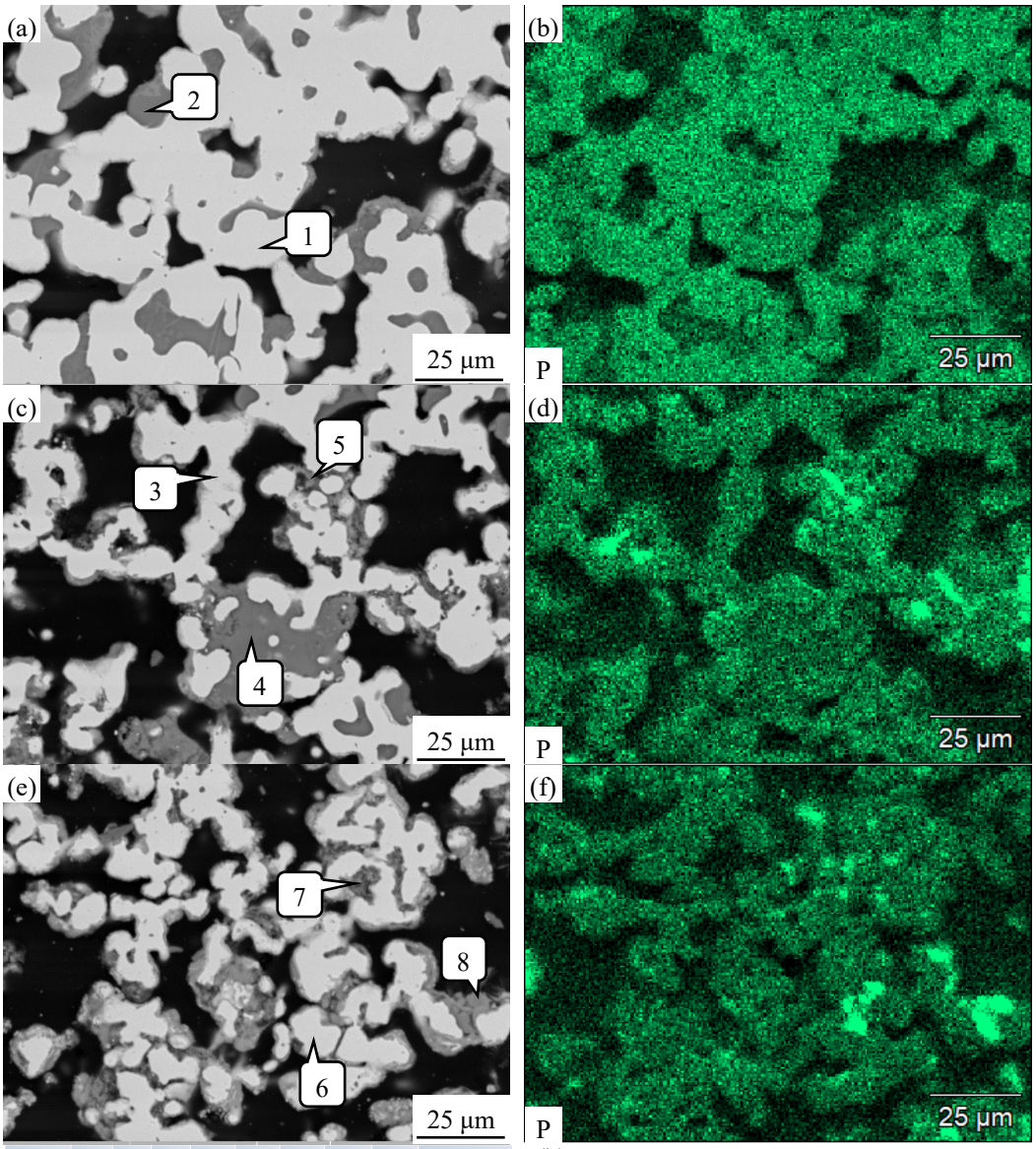

(g)

Points/ elements	O	Na	Al	Si	P	Ca	Fe	Total	Minerals
1	-	-	-	-	0.74	-	99.26	100.00	Metallic iron
2	59.02	-	13.54	19.46	0.41	7.57	-	100.00	Aluminosilicate
3	-	-	-	-	-	-	100.00	100.00	Metallic iron
4	40.50	1.78	-	8.76	4.54	44.42	-	100.00	Dicalcium silicate
5	21.00	-	-	-	18.77	46.27	13.96	100.00	Apatite
6	-	-	-	-	-	-	100.00	100.00	Metallic iron
7	40.73	3.31	-	11.98	4.52	39.46	-	100.00	Dicalcium silicate
8	34.55	-	-	-	19.56	45.89	-	100.00	Apatite

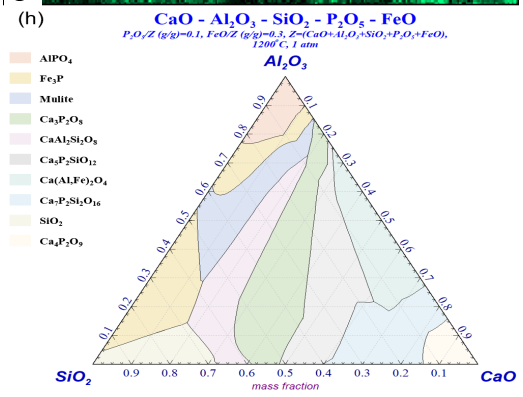

Fig. 7. Occurrence states of phosphorus in reduced products under different dosages of calcium carbonate and sodium carbonate: (a) 0%; (c) 9%; (e) 15%; (b), (d), (f) Respectively represent the phosphorus distributions in (a), (c), (e); (g) Mass percentages of each element from point 1 to point 8; (h) Phase diagram

-rals were not reduced, and calcium carbonate did not participate in the reaction. When the temperature rises to 900 °C, the contents of magnetite and calcite decrease to 34.10% and 22%, respectively, and there are diffraction peaks of wustite and lime, but no metallic iron peak is observed. When the temperature is further increased to 1000 °C, the diffraction peak of metallic iron appears in the reduction product,

and the content of wustite increases to 55.6%, while the content of magnetite decreases to 5.1%, indicating that most magnetite has been reduced to wustite, and a small amount of wustite is further reduced to metallic iron. When the temperature rises to 1100 °C, the reduction products are mainly composed of metallic iron and wustite, in which the content of metallic iron reaches 79.9% and that of wustite decreases to 3.6%. At 1200 °C, the content of metallic iron increased to 84.4%, and the content of wustite further decreased to 0.6%.

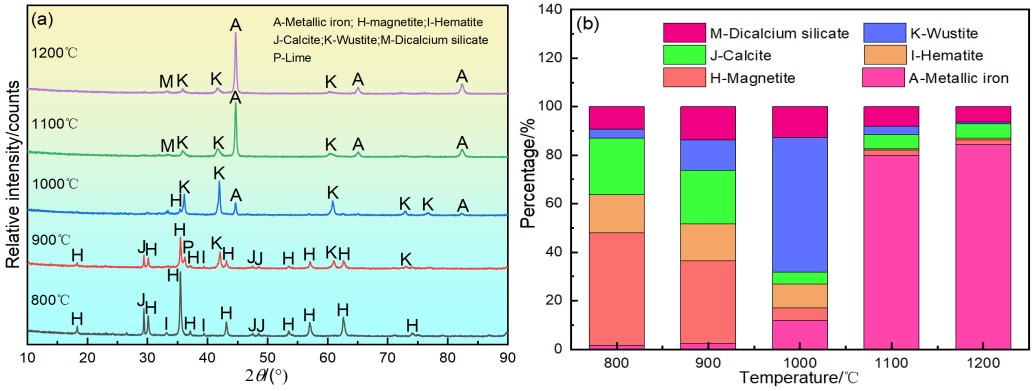

Fig. 8. Mineral ineral composition of reduced products at different temperatures: (a) Mineral composition; (b) Contents of different minerals

To investigate the effect of temperature on the occurrence state of phosphorus in the reduced products, the reduced products obtained at different temperatures were analyzed by SEM–EDS, and the results are shown in Fig. 9. When the temperature was below 900 °C, the structure of the high-phosphorus sample remained largely unchanged after reduction, and the magnetite contained phosphorus, indicating that the phosphorus in the iron minerals did not react. When the temperature was increased to 1000 °C, the structure of the reduced product began to change, and wustite contained phosphorus. At 1100 °C, the metallic iron particles were free of phosphorus, while phosphorus was present in wustite, apatite, and calcium silicate. This indicates that at temperatures below 1100 °C, part of the phosphorus in wustite remained unreacted. When wustite was reduced to metallic iron, part of the phosphorus in wustite reacted with calcite in the high-phosphorus sample to form apatite, and the other part entered calcium silicate, thus resulting in phosphorus-free metallic iron particles. When the reduction temperature was increased to 1200 °C, a new change in the occurrence state of phosphorus appeared: both metallic iron and wustite were free of phosphorus, and phosphorus existed in apatite and calcium silicate. This indicates that when the iron minerals were reduced to wustite, the phosphorus in them entered the gangue phase. It can also be observed that increasing the temperature promoted the formation and growth of metallic iron particles.

3.5. Transformation process of phosphorus under different reduction time

To clarify the relationship between phosphorus transformation in the iron minerals and iron reduction, the mineral composition of the reduced products obtained at different reduction time was analyzed by XRD, and the results are shown in Fig. 10. At a reduction time of 3 min, the reduced product mainly consisted of magnetite and calcite. When the reduction time is extended to 5 min, the content of magnetite decreases to 39.7%, that of calcite decreases to 8.6%, that of wustite increases to 38.3%, and metallic iron peaks appear, indicating that part of magnetite has been reduced to metallic iron. However, due to the short reduction time, there are still a considerable number of magnetite and wustite that have not been reduced. When the reduction time is 10 min, the content of wustite is 44.8%, the content of metallic iron increases to 48.2%, and magnetite basically disappears. When the roasting time was 30 min, the diffraction peak of dicalcium silicate appeared, and the content of wustite decreased to 14.1%, while the content of metallic iron increased to 76.1%, indicating that the metallic iron produced increased with the roasting time.

The reduced products obtained at different reduction time were analyzed by SEM–EDS, and the results are shown in Fig. 11. At a reduction time of 3 min, the structure of the reduced product did not

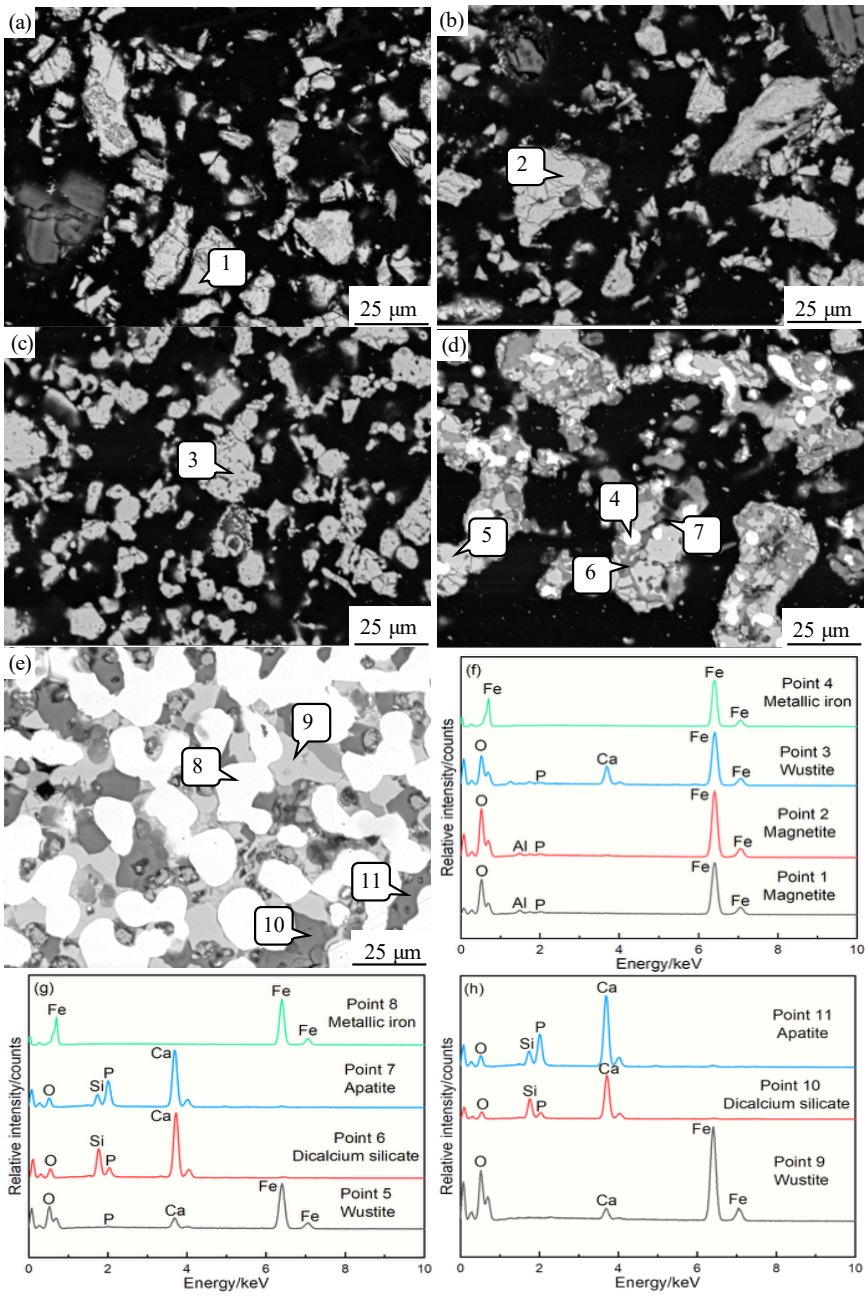

Fig. 9. Occurrence states of phosphorus in reduced products at different temperatures: (a) 800 ℃; (b) 900 ℃; (c) 1000 ℃; (d) 1100 ℃; (e) 1200 ℃; (f)~(h) Energy spectra of points 1 to 11

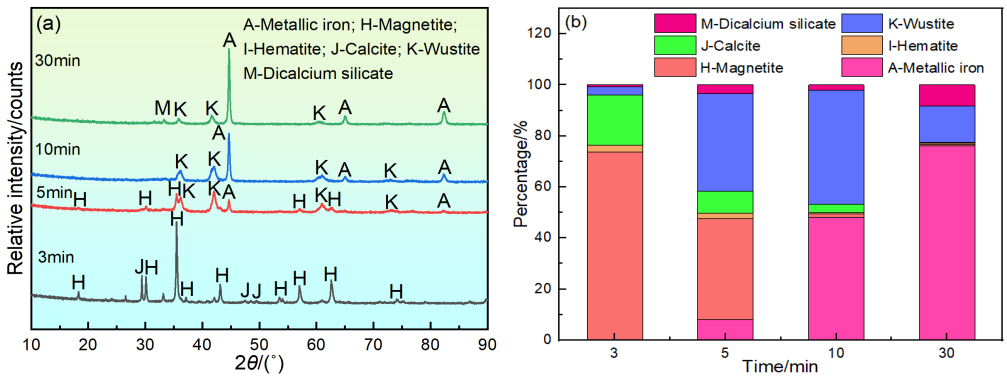

Fig. 10. Mineral composition of reduced products at different time: (a) Mineral composition; (b) Quantitative analysis of different minerals

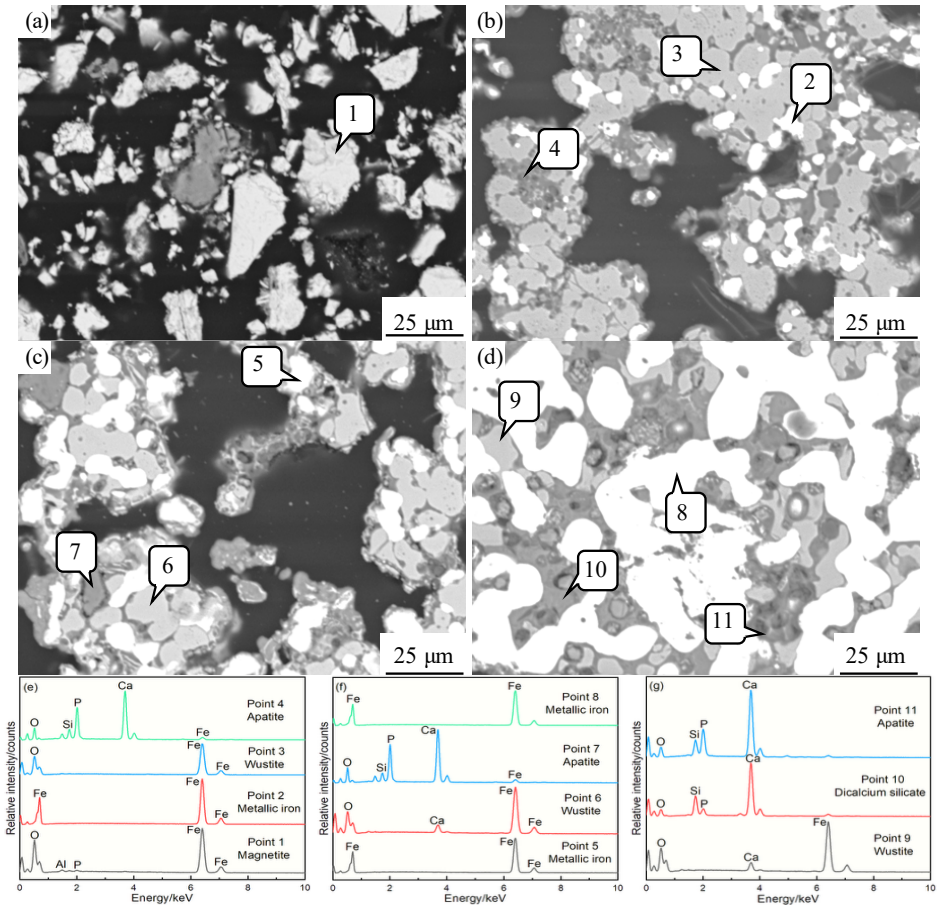

Fig. 11. Phosphorus distribution maps of reduced products at different time: (a) 3 min; (b) 5 min; (c) 10 min; (d) 30 min; (e)~(g) Energy spectra of points 1 to 11

change, and magnetite contained phosphorus, indicating that phosphorus did not react when hematite was reduced to magnetite and that the phosphorus in magnetite remained unreacted. At a reduction time of 5 min, the structure of the reduced product began to change, and fine metallic iron particles appeared. Both metallic iron and wustite were free of phosphorus, while phosphorus was present in apatite. This indicates that when magnetite was reduced to wustite, the phosphorus in the iron minerals reacted with calcite in the high-phosphorus sample to form apatite. When the reduction time was extended to 30 min, neither metallic iron nor wustite contained phosphorus. The formation of calcium silicate consumed silica, preventing the reduction of the apatite that had formed, and the metallic iron particles grew further. Based on the above results, the transformation process of phosphorus from iron minerals during reduction using calcium carbonate and sodium carbonate as dephosphorization agents is shown in Fig. 12.

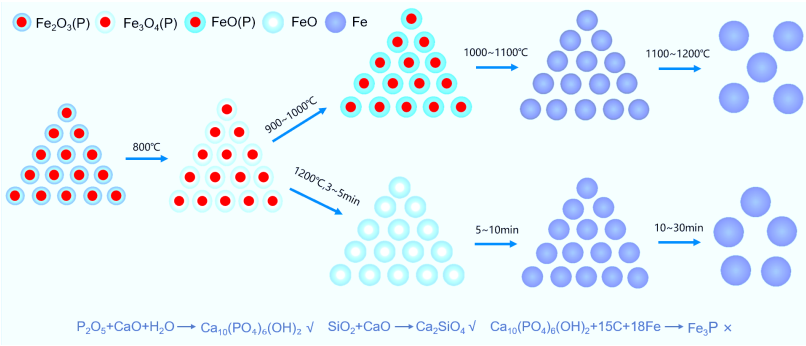

Fig. 12. Transformation process of phosphorus in iron minerals during the reduction process by calcium carbonate and sodium carbonate

4. Conclusions

(1) The addition of calcium carbonate and sodium carbonate reacts with the silicon components in the high-phosphorus sample to form calcium silicate, preventing the reduction of the apatite that has been formed.
(2) Increasing the proportion of sodium carbonate in the dephosphorization agent does not change the occurrence state of phosphorus, but it makes the boundary between apatite and metallic iron clearer, which promotes the liberation of metallic iron grains during the grinding stage.
(3) When the reduction temperature is between 1000 °C and 1100 °C, phosphorus enters the gangue during the reduction of wustite to metallic iron. When the temperature is raised to 1200 °C, phosphorus in the iron minerals enters the gangue phase when the iron minerals are reduced to wustite.
(4) All of the phosphorus in the iron minerals enters the gangue phase within 5 min, and further extending the time promotes the formation of metallic iron and the growth of metallic iron particles.

Acknowledgements

The authors would like to thank the Yunnan Fundamental Research Projects (202501CF070154), the Guangxi Regional Innovation Capability Enhancement Plan (GuiKeXT2504240005), the Open Project of the National Key Laboratory of New Technologies for Enhanced Metallurgy of Nonferrous Metals (YSQH-ZD-25003) and the Yunnan Fundamental Research Projects (202501BN070001-013, 202401BE070001-032) for the financial support.

References

DING H. Y., YUAN S., GAO P., et al. 2023. *Research on efficient utilization of high-phosphorus oolitic hematite for iron enrichment and dephosphorization by hydrogen mineral phase transformation*. J. Cent. South Univ. 30(12), 4021–4035.

DONG S. S., LI T., YU J. M., et al. 2024. *A strategy for treatment of low-grade ore: Efficient separation and purification of iron*. Process Saf. Environ. Prot. 191, 1313–1323.

GUO L., GAO J. T., ZHONG Y. W., et al. 2015. *Phosphorus removal of high-phosphorus oolitic iron ore with acid-leaching fluidized-reduction and melt-separation process*. ISIJ Int. 55(9), 1806–1815.

HU M. J., ZHU D. Q., PAN J., et al. 2026. *Reduction and migration behavior of phosphorus in coal-based reduction of high-phosphorus oolitic iron ore*. J. Iron Steel Res. Int. 33, 78.

JIA Y., RUAN R. M., QU J. K., et al. 2024. *Multi-scale and trans-disciplinary research and technology developments of heap bioleaching*. Minerals 14(8), 808.

JI G. H., GAO X., SOHN I. L., et al. 2025. *In-situ observation of dissolution behavior and kinetics of fluorapatite particles in high-phosphorus iron ores*. Sep. Purif. Technol. 358, 130301.

JI G. H., GAO X., SOHN I. L., et al. 2025. *Review of beneficiation techniques and new thinking for comprehensive utilization of high-phosphorus iron ores*. Miner. Eng. 223, 109176.

LI W. B., YU Y. S., WANG M. X., et al. 2025. *Efficient iron recovery and dephosphorization from high-phosphorus oolitic iron ore: Process optimization and mineralogy*. J. Environ. Chem. Eng. 13(5), 118121.

LIU F., ZHANG Y. C., ZENG W., et al. 2025. *Iron recovery and dephosphorization behaviors from high-phosphorus oolitic hematite by gas-based direct reduction and magnetic separation*. J. Iron Steel Res. Int. 32(3), 550–563.

LIU M. X., ZHANG H. M., CHEN T. J., et al. 2026. *Comparative study of magnetic reduction–separation behavior and kinetics of refractory oolitic iron ore through coal-based versus gas-based reductive roasting*. J. Iron Steel Res. Int. 33, 128.

POWNCEBY M. I., HAPUGODA S., MANUEL J., et al. 2019. *Characterisation of phosphorus and other impurities in goethite-rich iron ores–Possible P incorporation mechanisms*. Miner. Eng. 143, 106022.

SILVA L. M., GIESE E. C., MEDEIROS G. A., et al. 2022. *Evaluation of the use of Burkholderia caribensis bacteria for the reduction of phosphorus content in iron ore particles*. Mater. Res. 25, e20210427.

SINGH A., SINGH V., PATRA S., et al. 2024. *Review on high phosphorus in iron ore: Problem and way out*. Mining Metall. Explor. 41(3), 1497–1507.

WANG X. P., LU W. D., RONG L. K., et al. 2025. *Red mud as a green dephosphorization agent: Co-reduction with high-phosphorus oolitic hematite for iron extraction and dephosphorization*. Process Saf. Environ. Prot. 193, 990–1001.

WU S. C., LI Z. Y., SUN T. C., et al. 2021. *Effect of additives on iron recovery and dephosphorization by reduction roasting-magnetic separation of refractory high-phosphorus iron ore*. Int. J. Min. Met. Mater. 28(12), 1908–1916.

WU S. C., LIU S. R., LI B., et al. 2026. *Effect of calcium carbonate on transformation behavior of phosphorus in iron minerals during direct reduction*. J. Iron Steel Res. Int. 33, 207.

WU S. C., SUN T. C., KOU J. 2022. *A novel and clean utilization of converter sludge by co-reduction roasting with high-phosphorus iron ore to produce powdery reduced iron*. J. Clean. Prod. 363, 132362.

WU S. C., SUN T. C., KOU J., et al. 2023. *A new iron recovery and dephosphorization approach from high-phosphorus oolitic iron ore via oxidation roasting-gas-based reduction and magnetic separation process*. Powder Technol. 413, 118043.

XIAO J. H., ZHOU L. L. 2019. *Increasing iron and reducing phosphorus grades of magnetic-roasted high-phosphorus oolitic iron ore by low-intensity magnetic separation–reverse flotation*. Processes 7(6), 388.

YE F. P., DUAN Y. J., GUO Z. Q. 2024. *Experimental investigation on magnetic-gravity combined beneficiation of low-grade iron ore*. Physicochem. Probl. Miner. Process. 60(5), 192832.

YOU J. X., ZHANG S. H., WU S. C., et al. 2024. *Preparation of reduced iron powder from high-phosphorus iron ore: A pilot-scale rotary-kiln investigation*. Miner. Process. Extr. Metall. Rev. 45(6), 644–653.

YU K. X., ZOU W. J., KOU J., et al. 2025. *Mechanism of organic/inorganic components of reducing agent in direct reduction roasting of high-phosphorus oolitic hematite*. J. Cent. South Univ. 56(4), 1275–1289.

ZHANG X. L., CHENG S. K., GAO P., et al. 2025. *Unlocking iron from oolitic hematite: Clean mineral phase transformation for primary iron concentrate production*. Process Saf. Environ. Prot. 200, 107377.

ZHAO L. D., WU D. Y., YOU X. M., et al. 2024. *Dephosphorization of high-phosphorus iron ore by direct reduction of hydrogen-rich gases and melting separation*. J. Cent. South Univ. 31(11), 4120–4136.

ZHAO Y. J., LI G. Q., LI J. B., et al. 2026. *Preparation of phosphorus-rich iron via hydrogen reduction–melting separation of high-phosphorus oolitic hematite*. J. Iron Steel Res. Int. 33, 208.

ZHOU Z. Y., ZHANG X. L., LI W. B., et al. 2024. *An innovation for strengthen iron extraction from phosphorus-bearing refractory iron ore via suspension magnetization roasting and flotation*. Adv. Powder Technol. 35(4), 104382.

ZHU D. Q., CHUN T. J., PAN J., et al. 2013. *Upgrading and dephosphorization of Western Australian iron ore using reduction roasting by adding sodium carbonate*. Int. J. Min. Met. Mater. 20(6), 505–513.